Supplementary information

Feedback attribution to recent Arctic temperature extremes and the role of natural variability

Blau et al.

This PDF file includes:

Figures S1 to S13
Table S1

Figure S1: Spatial map of surface temperature anomalies in extreme years from different reanalysis products

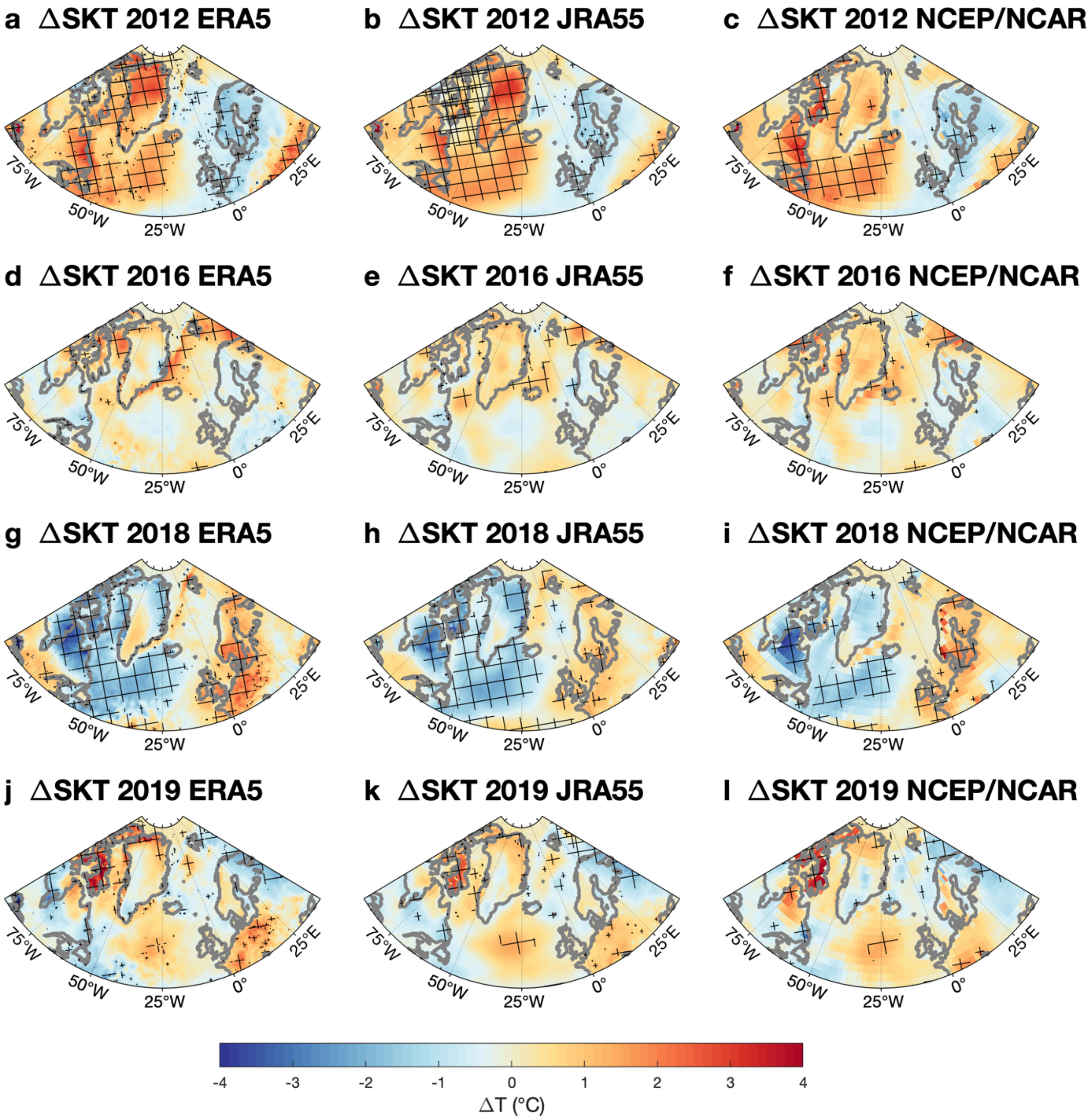

The detrended anomalies of surface temperature from ERA5 (a), JRA-55 (b), and NCEP/NCAR (c) in the year 2012. The second, third, and fourth rows illustrate 2016, 2018, and 2019 values, respectively. The hatches indicate where the anomalies are outside the 90th percentile.

Figure S2: Climate trends from 1979 to 2021 from ERA5

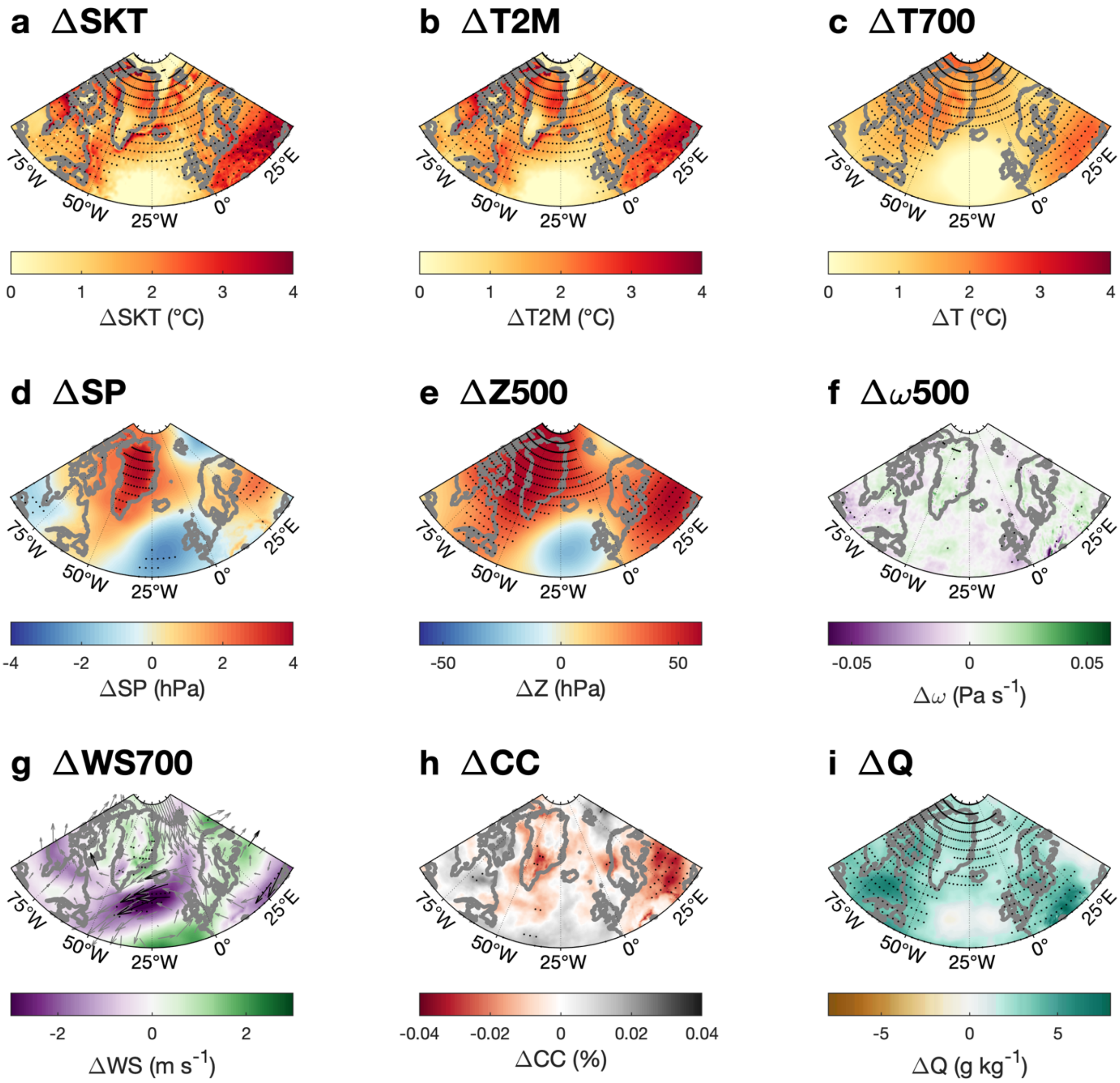

The trends of different variables from ERA5. The figure shows the trend of surface temperature (a), near-surface temperature (b), air temperature at the 700 hPa pressure surface (c), the surface pressure (d), the geopotential height (e) and the vertical velocity at the 500 hPa pressure surface (f), the wind circulation and speed at the 700 hPa pressure surface (g), and the mean cloud cover (h) and vertically integrated specific humidity (i) between the 1000 hPa and the 200 hPa pressure surface. The values depict trends from 1979 to 2021. Stippling indicates significant trends based on a 95 % confidence interval.

Figure S3: Spatial relationship between Greenland surface temperature and feedback processes

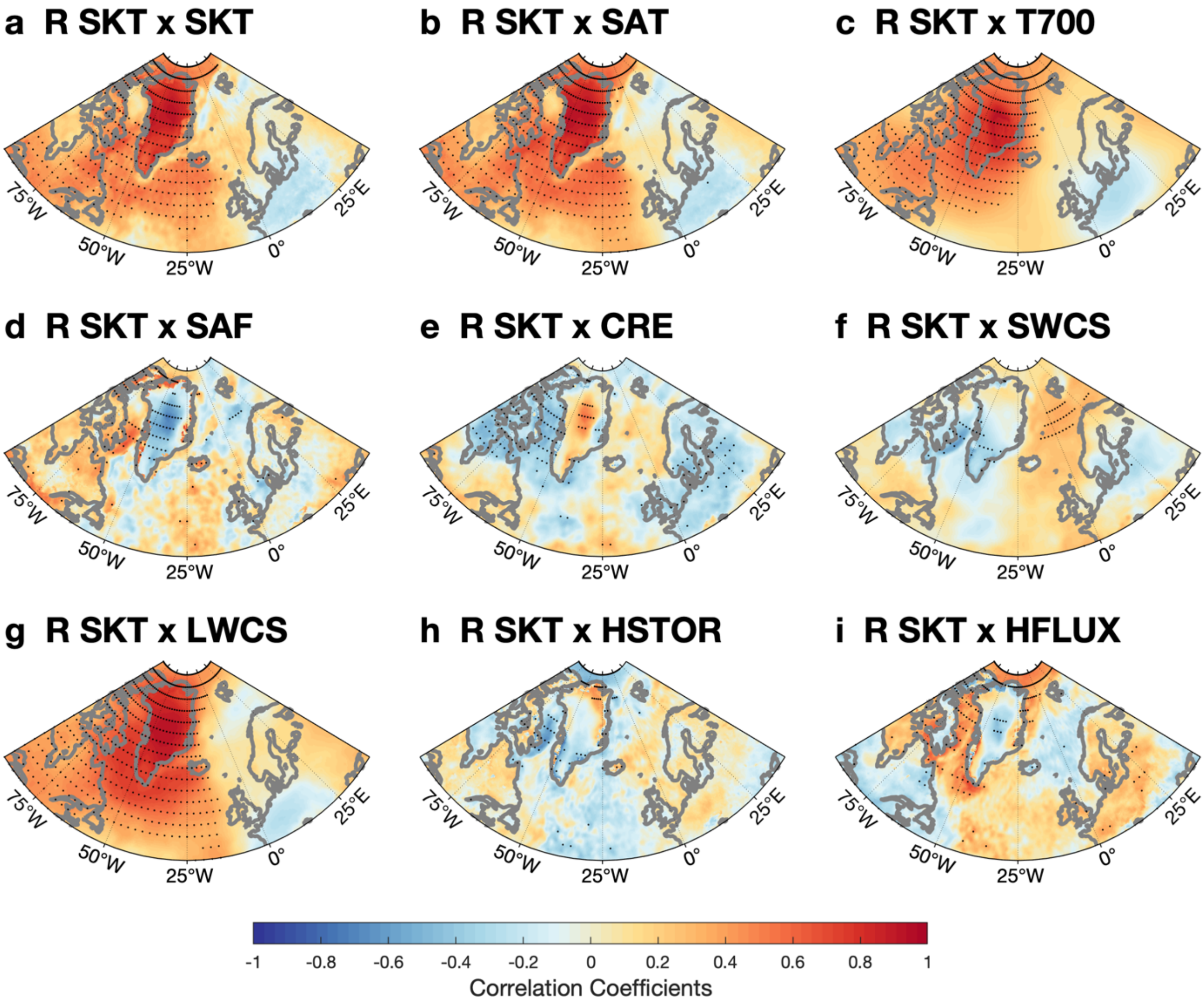

Correlation coefficients of Greenland surface temperature and other variables. The relationship based on Pearson's correlation coefficients and is calculated for surface temperature (a), near-surface temperature (b), air temperature at the 700 hPa pressure surface (c), the surface albedo feedback (d), the cloud radiative effect (e), the clear-sky net shortwave radiation (f), the clear-sky downwelling longwave radiation (g), the heat storage term (h), and the turbulent heat fluxes (i). Stippling indicates significant correlations based on a 95 % confidence interval.

Figure S4: Feedback attribution, clear-sky longwave radiation anomalies in extreme years from different reanalysis products

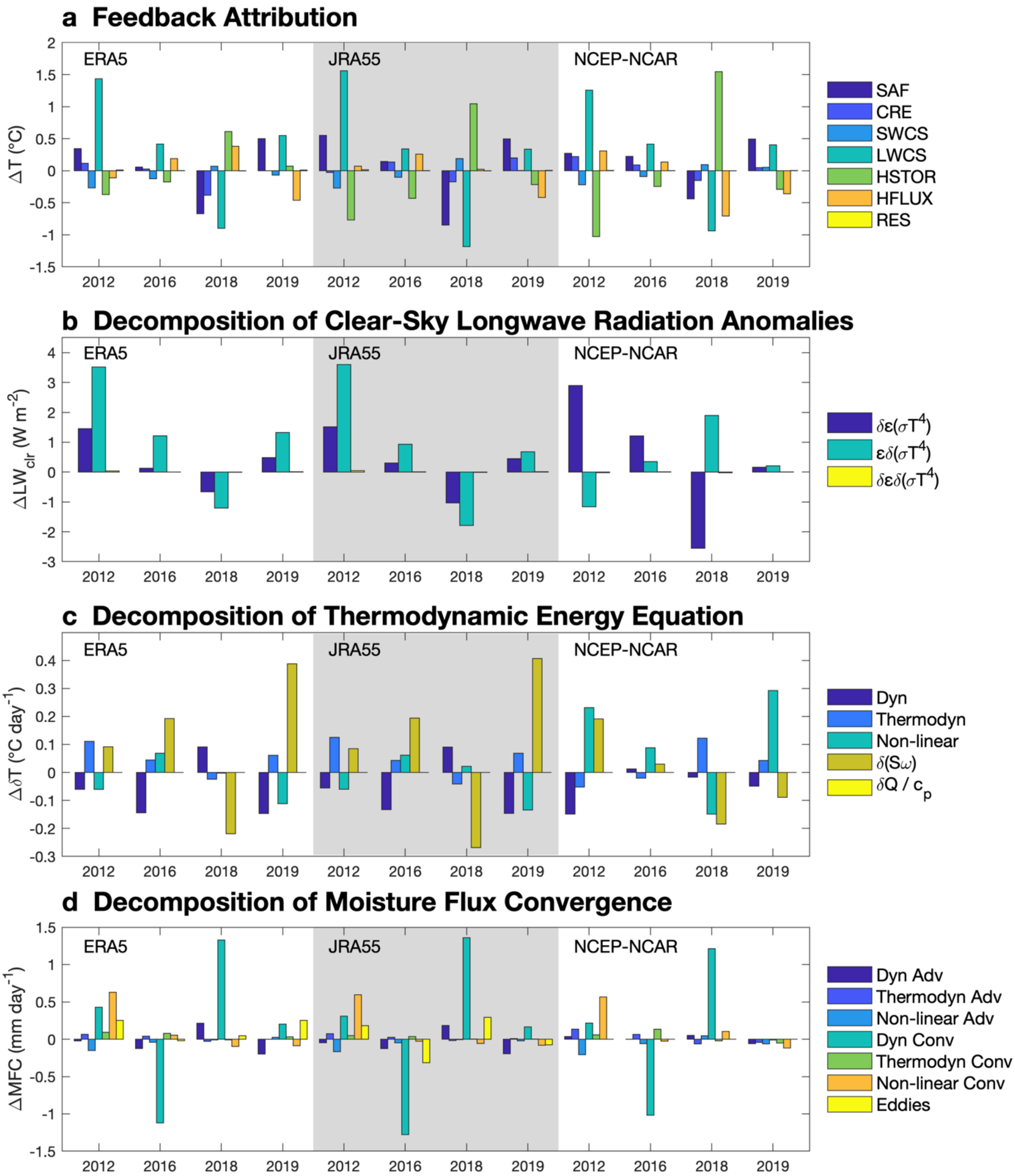

The feedback decomposition (a), the decomposition of clear-sky downwelling longwave radiation (b), and the results of the thermodynamic energy equation (c) and moisture flux convergence (d) were calculated from outputs of different reanalysis datasets. The figure illustrated only the results for the extreme temperature summers of 2012, 2016, 2018, and 2019.

Figure S5: Mapped results of the thermodynamic energy equation

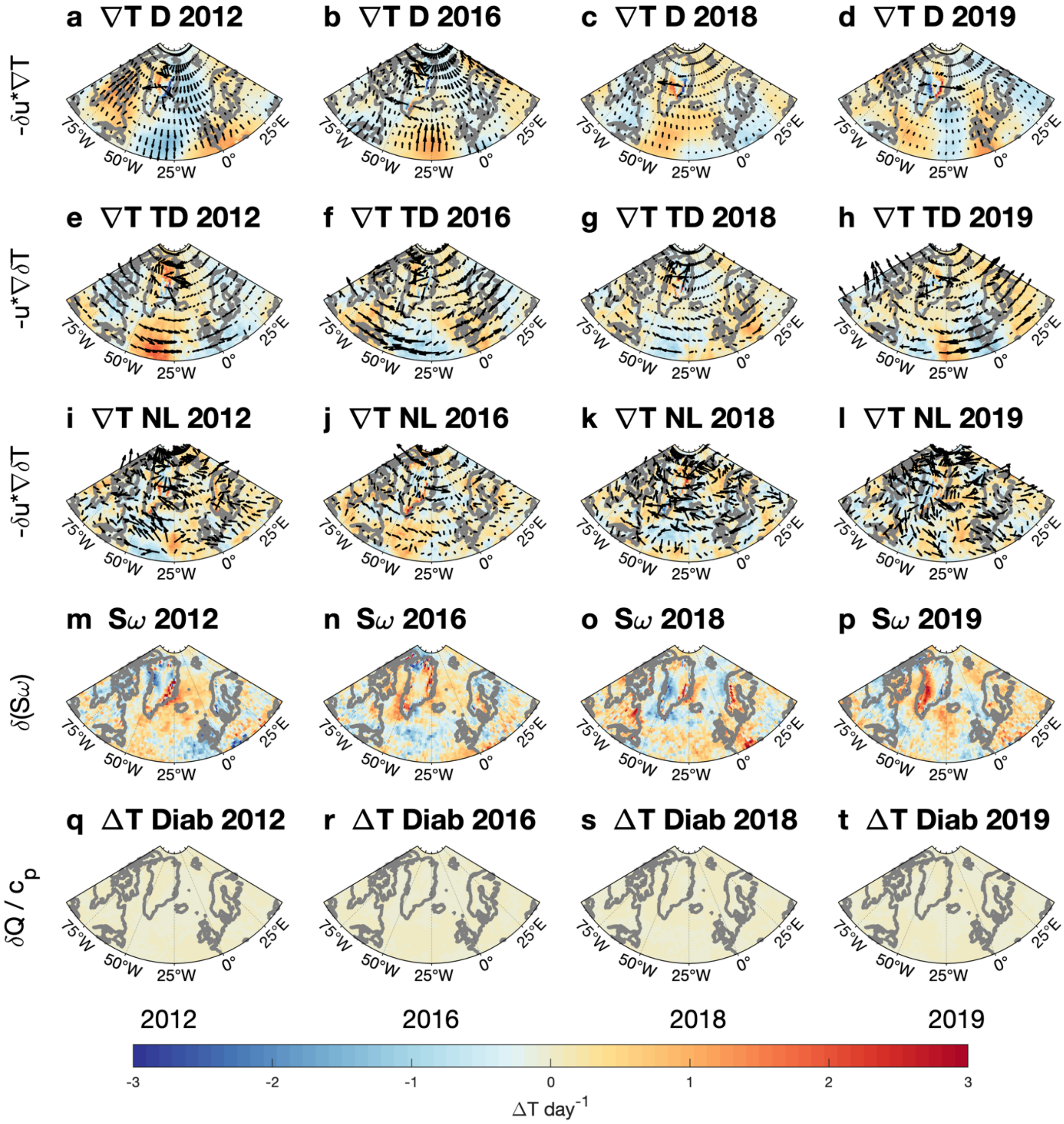

The thermodynamic energy equation for the 700 hPa pressure surface. Maps illustrated the grid-by-grid calculated results of dynamic (first row), thermodynamic (second row), and non-linear (third row) temperature advection, the static stability term (fourth row), and the diabatic heating (fifth row). Values presented are from extreme years 2012, 2016, 2018, and 2019.

Figure S6: Mapped results of the anomalous moisture flux convergence

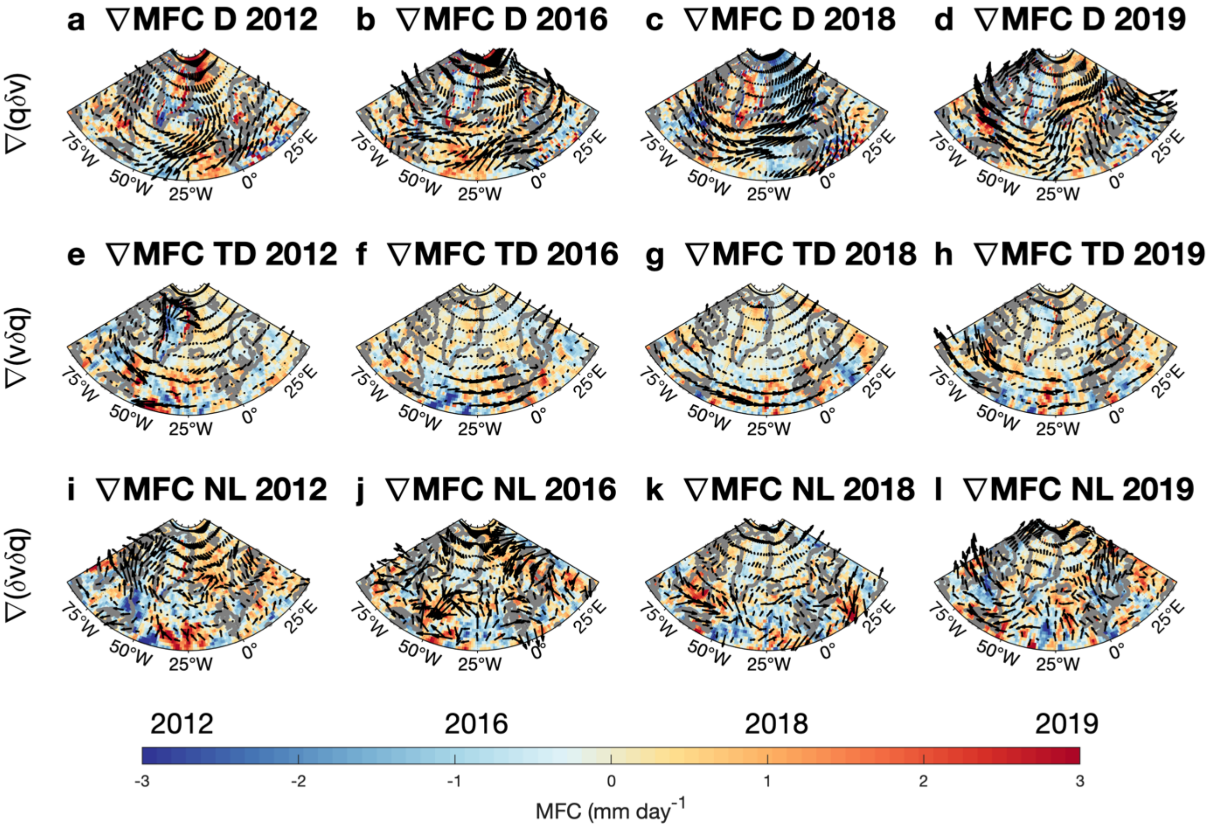

The vertically integrated anomalous moisture flux convergence. Maps illustrated the grid-by-grid calculated results of dynamic (first row), thermodynamic (second row), and non-linear (third row) moisture flux convergence anomalies.

Figure S7: Ocean heat transport

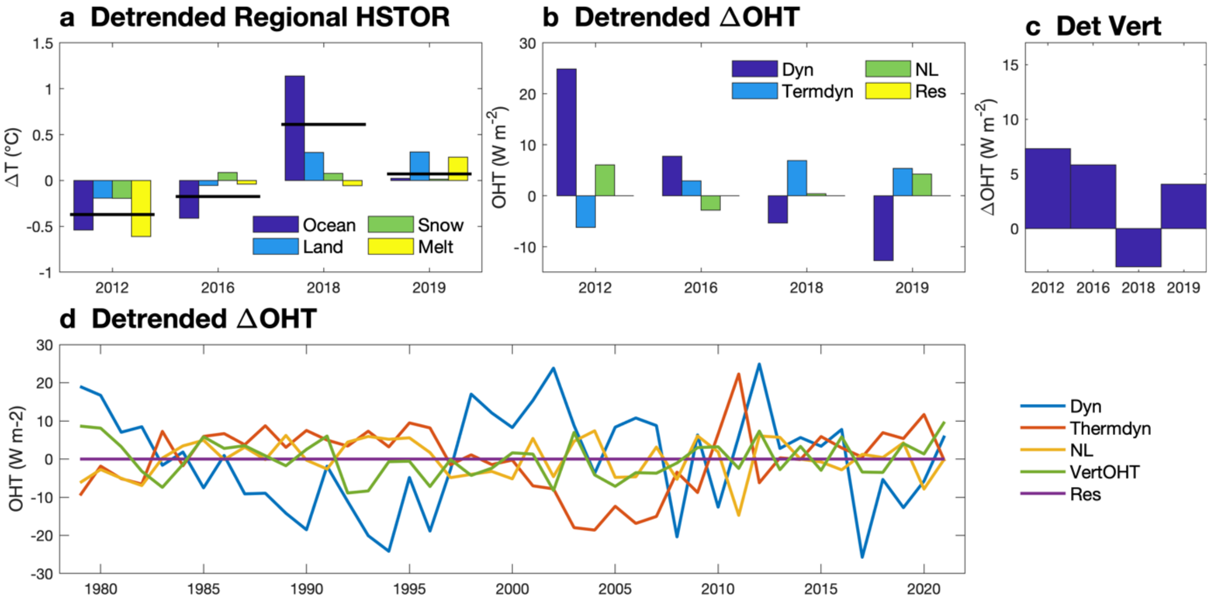

The ocean heat transport as mean over the ocean gridpoints in the Greenland domain. The heat storage term was split into ocean gridpoints (47.32 %), land gridpoints (13.78 %), snow gridpoints (36.30 %), and gridpoints in which snow starts to melt (SKT = 273.15) (2.60 %) (a). In the ocean gridpoints beside the net energy balance, energy convergence/divergence was calculated (b). The vertical component is in (c) with positive values in a downward direction. (d) shows detrended timeseries.

Figure S8: Regressed partial temperature contributions of feedback processes

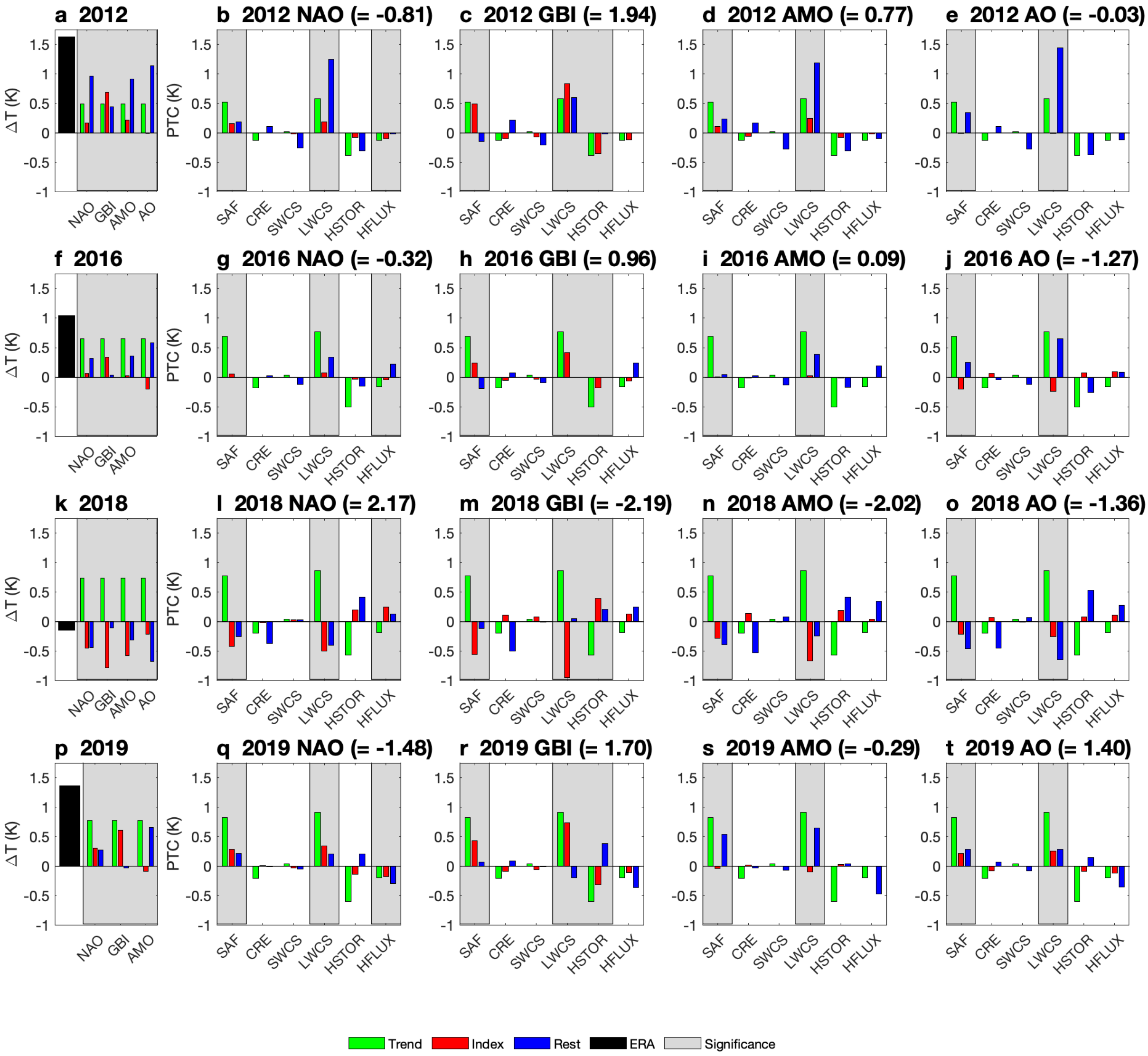

Regression analysis of the surface energy balance feedbacks against the North Atlantic oscillation, the Greenland blocking index, the Atlantic multi-decadal oscillation, and the Arctic oscillation in the extreme years 2012 (first row), 2016 (second row), 2018 (third row), and 2019 (fourth row). The related correlation coefficients are in Table S1.

Figure S9: Partial correlation of different climate indices with surface temperature anomalies from different reanalysis products

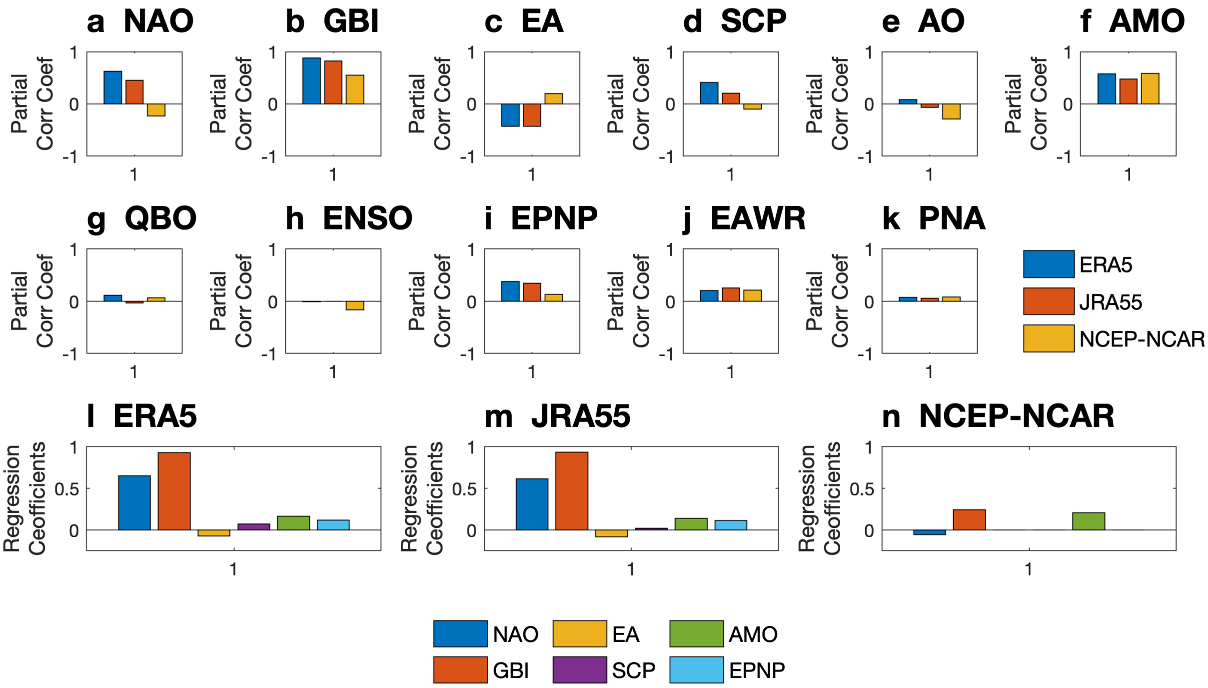

The partial correlation and regression coefficients connect climate indices to surface temperature anomalies. The partial correlation coefficients are calculated for ERA5, JRA-55, and NCEP-NCAR reanalysis products between surface temperature and the North Atlantic oscillation (a), the Greenland blocking index (b), the East Atlantic pattern (c), the Scandinavian pattern (d), the Arctic oscillation (e), the Atlantic multi-decadal oscillation (f), the Quasi-biennial oscillation (g), the El Niño Southern oscillation (h), the East Pacific/North Pacific pattern (i), the East Atlantic/West Russia pattern (j), and the Pacific North America pattern (k). The regression coefficients for indices with significant partial correlation are in for ERA5 (l), for JRA-55 in (m), and for NCEP-NCAR in (n). We used lasso regression to fit the multivariate regression model.

Figure S10: Spatial maps of multivariate regression coefficients

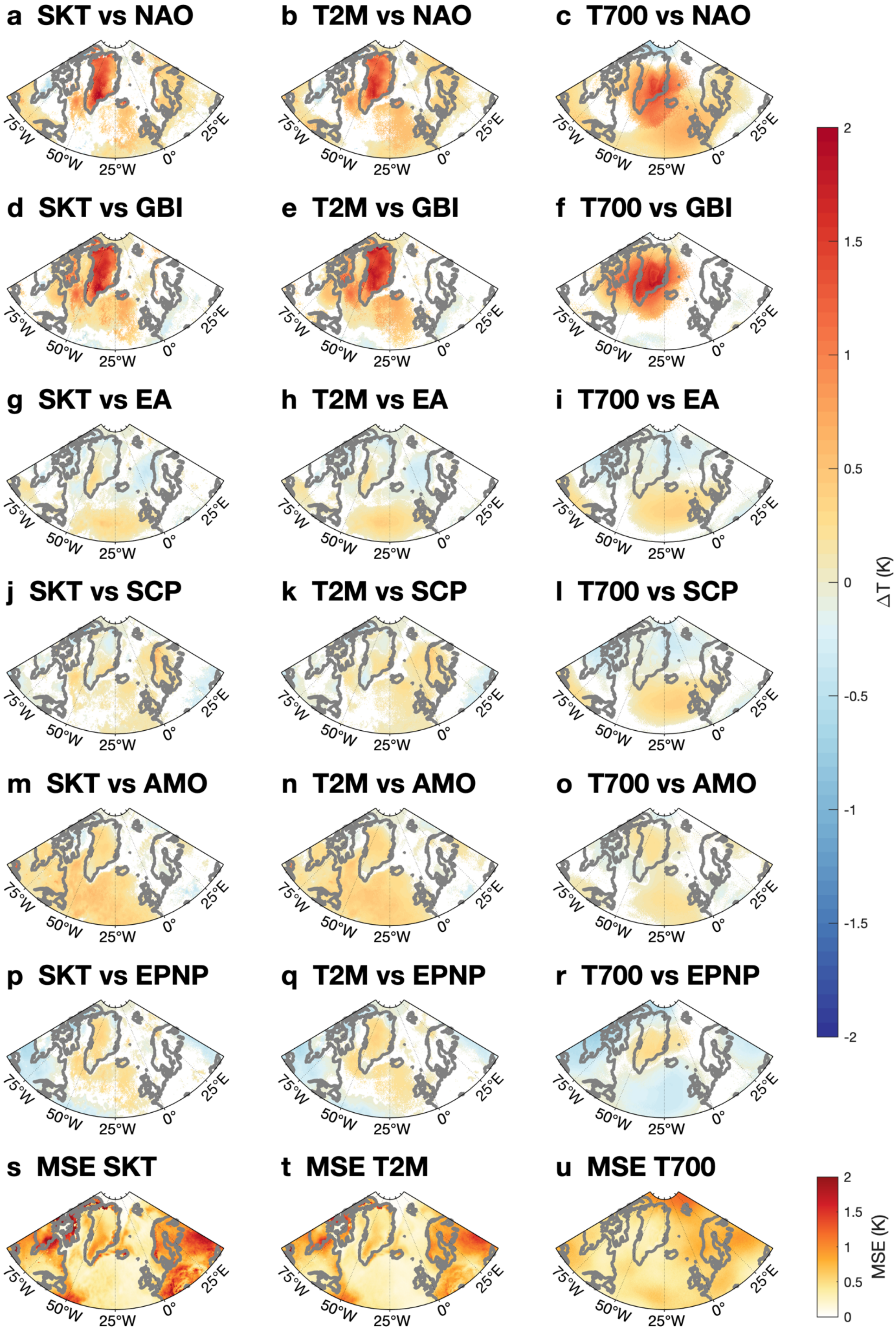

The grid-by-grid calculated regression coefficients were calculated using lasso regression. The predictors are the North Atlantic oscillation (first row), the Greenland blocking index (second row), the East Atlantic pattern (third row), the Scandinavian pattern (fourth row), the Atlantic multi-decadal oscillation (fifth row), and the East Pacific/North Pacific pattern (sixth row). All indices share a significant partial correlation with surface temperature anomalies. The models were fitted to calculate surface temperature anomalies (a), near-surface temperature anomalies (b), and the temperature anomalies at the 700 hPa pressure surface (c) for each index, respectively. The bottom row shows the mean square error of the multivariate regression models for surface temperature anomalies (s), near-surface temperature anomalies (t), and the temperature anomalies at the 700 hPa pressure surface (u).

Figure S11: Spatial distribution of partial correlation coefficients

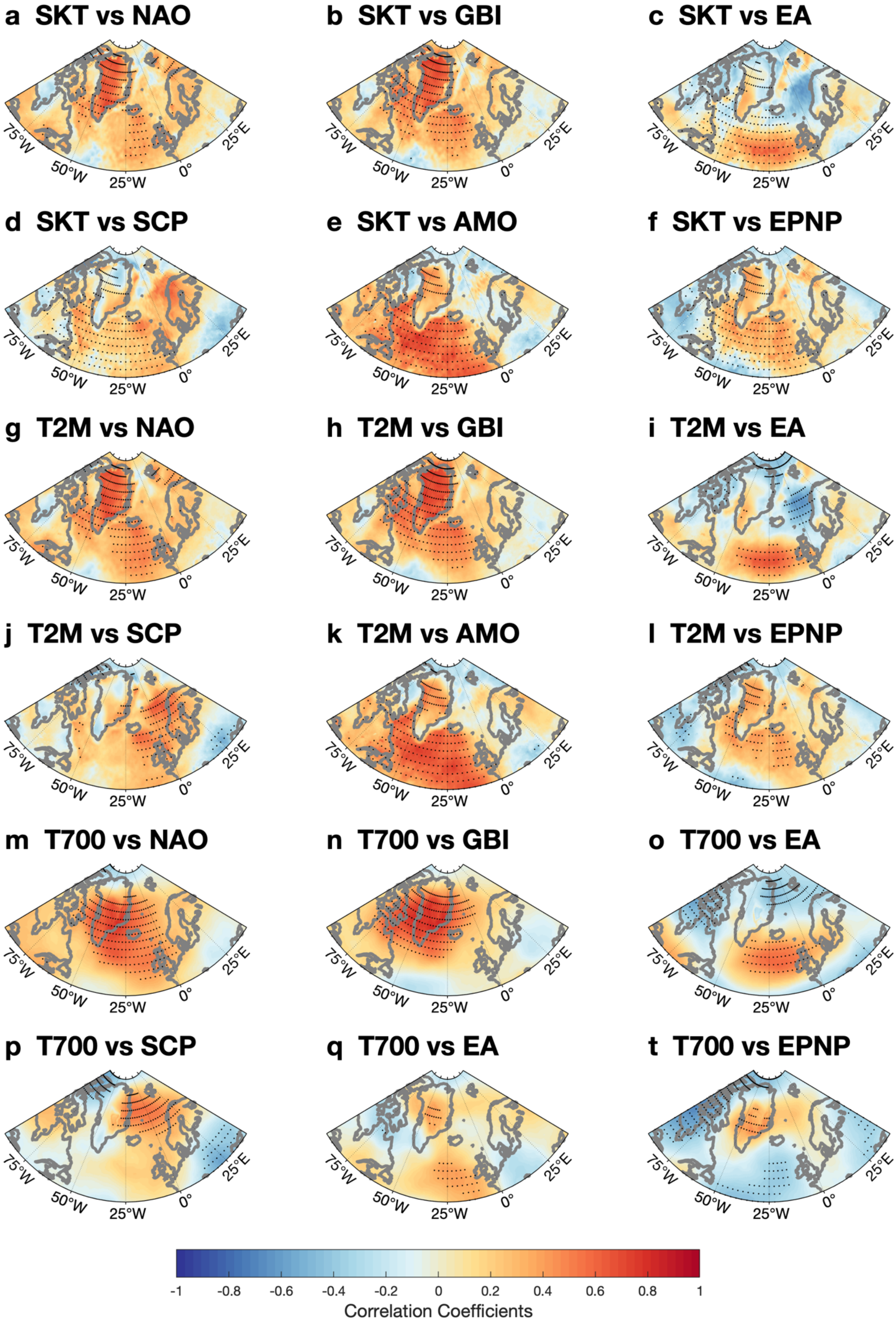

The spatial maps of grid-by-grid calculated partial correlation coefficients between climate indices and temperature anomalies. The partial correlation was calculated for surface temperature anomalies and the North Atlantic oscillation (a), the Greenland blocking index (b), the East Atlantic pattern (c), the Scandinavian pattern (d), the Atlantic multi-decadal oscillation (e), and the East Pacific/North Pacific pattern (f). The partial correlation is also calculated for the indices and the near-surface temperature anomalies (g-l) and temperature anomalies at 700 hPa pressure surface (m-t). The stippling indicates significant correlation coefficients based on a 95 % confidence interval.

Figure S12: Climate trends of blocking indicators

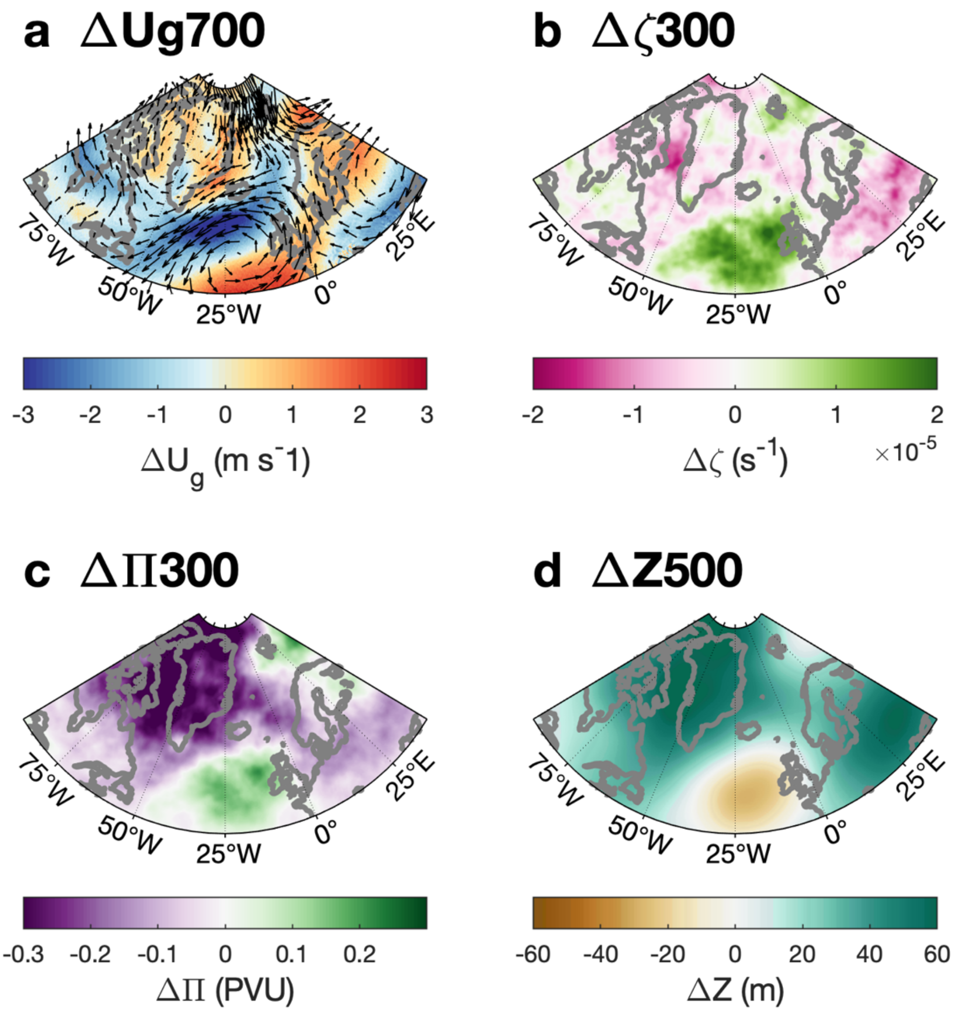

The trends in the geostrophic wind circulation (a), the relative vorticity (b), and potential vorticity (c) at the 300 hPa pressure surface, and the geopotential height (d) at the 500 hPa pressure surface. The trends are calculated from 1979 to 2021 from ERA5.

Figure S13: Comparison of the surface energy output from different reanalysis products

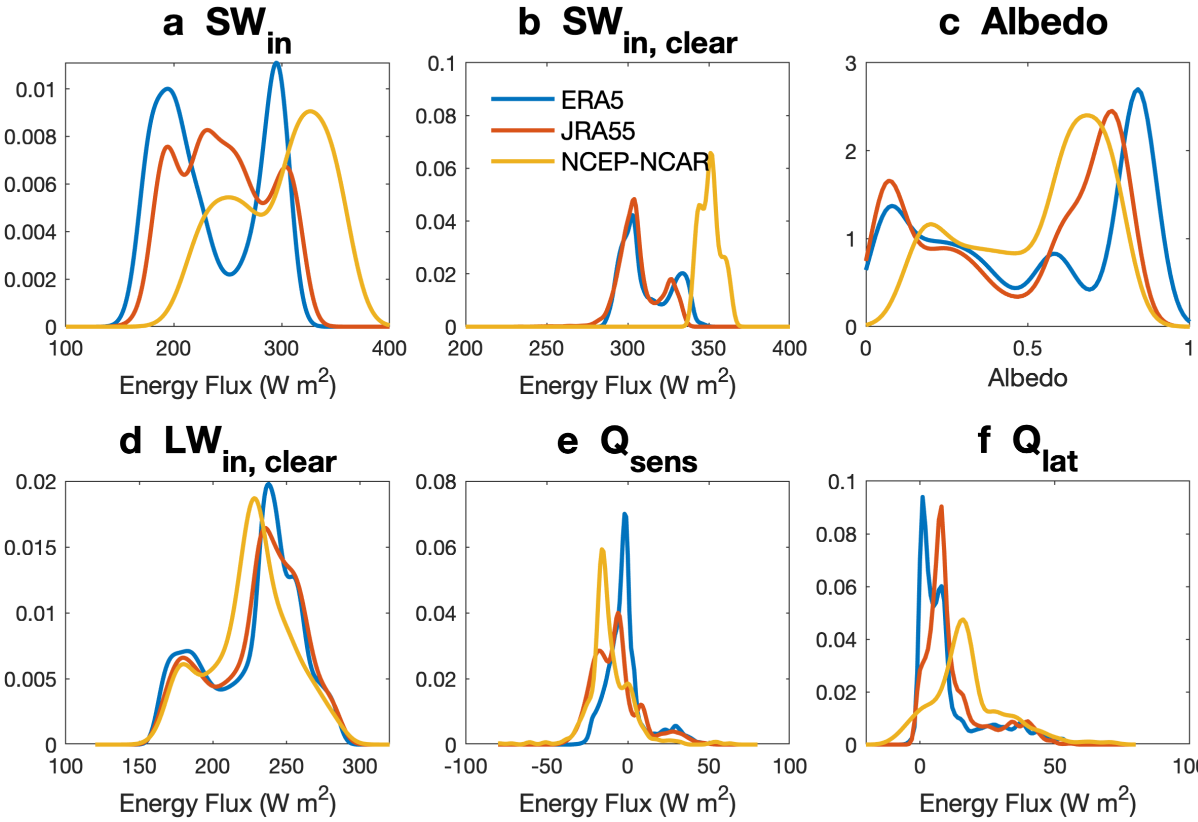

Kernel density distribution of surface energy variables from ERA5, JRA-55, and NCEP-NCAR. The robustness of surface energy fluxes was tested for the downwelling solar radiation (a), the clear-sky downwelling solar radiation (b), the surface albedo (c), the clear-sky downwelling longwave radiation (d), the sensible heat flux (e), and the latent heat flux (f). The distribution considers the summer mean values of each gridpoint in the Greenland domain.

Table S1: Correlation coefficients between climate indices and partial temperature contributions

	SKT	SAF	CRE	SWCS	LWCS	HSTOR	HFLUX
NAO	-0.40 *	-0.43 *	-0.02	0.10	-0.38 *	0.22	0.38 *
GBI	0.70 *	0.57 *	-0.17	-0.20	0.72 *	-0.43 *	0.20
AMO	0.56 *	0.31 *	-0.24	0.02	0.54 *	-0.23	-0.06
AO	0.30 *	0.35 *	-0.17	0.02	0.30 *	-0.14	-0.26

[+] Abbreviations: Surface temperature (SKT), surface albedo feedback (SAF), cloud radiative effect (CRE), clear-sky net shortwave radiation (SWCS), clear-sky downwelling longwave radiation (LWCS), heat storage (HSTOR), turbulent heat fluxes (HFLUX)

[-] Abbreviations: North Atlantic oscillation (NAO), Greenland blocking index (GBI), Atlantic multi-decadal oscillation (AMO), Arctic oscillation (AO)